1 Spatio-temporal variability of the carbonate system and air-sea $CO_2$ fluxes in the

2 South Yellow Sea and East China Sea during the warm seasons

3

4 Xue Deng[1,2], Gui-Ling Zhang[1,2], Ming Xin[2,3], Chun-Ying Liu[1,2,*], Wei-Jun Cai[4]

5

6 [1] Key Laboratory of Marine Chemistry Theory and Technology, Ministry of Education,

7 Qingdao 266100, PR China

8 [2] Laboratory for Marine Ecology and Environmental Science, Qingdao National

9 Laboratory for Marine Science and Technology, Qingdao 266071, PR China

10 [3] Key Laboratory for Marine Bioactive Substances and Modern Analytical

11 Technology, the First Institute of Oceanography, Ministry of Natural Resources,

12 Qingdao 266061, PR China

13 [4] School of Marine Science and Policy, University of Delaware, Newark, DE 19716,

14 United States

15 *Corresponding author: roseliu@ouc.edu.cn

16

17 **Key Points:**

18 • Strong $CO_2$ sinks turned into weak sources in the entire study area from spring

19 to summer

20    • The study area was divided into three subregions to separately examine the

21      driver mechanisms of the $p\text{CO}_2$ variations

22    • The $p\text{CO}_2$ variability was controlled by the combined influences of

23      temperature, biological activity and physical mixing

24

25    **Abstract**

26      Due to the complex physical and biogeochemical conditions, the adjacent South

27    Yellow Sea (SYS) and East China Sea (ECS) are ideal sites for studying different

28    carbonate characteristics in marginal seas. The distributions of carbonate system

29    parameters were investigated in this region in early spring and summer. Overall,

30    dissolved inorganic carbon (DIC) and alkalinity concentrations in the SYS were

31    higher than those in the ECS due to the Yellow River runoff which was featured with

32    intensive carbonate weathering and erosion. Low DIC, alkalinity and high pH values

33    were observed in the Zhe-Min Coastal Current with intensive primary production in

34    spring caused by the Changjiang River and Taiwan Warm Current. Temperature and

35    biological activities were the primary drivers in controlling the partial pressure of $\text{CO}_2$

36    ($p\text{CO}_2$) variability in the SYS, whereas temperature was the only dominant factor in

37    the outer shelf of the ECS, which was heavily impacted by the Kuroshio Current. The

38    $p\text{CO}_2$ dynamics was controlled by primary production and physical mixing in the

39    Changjiang River plume and the inner and middle shelves of the ECS, due to the

40    influence of the Changjiang River with high nutrient supply. Overall, strong $\text{CO}_2$

41    sinks (-4.11 ± 5.28 mmol $\text{m}^{-2}\text{d}^{-1}$) turned into weak sources (0.88 ± 5.09 mmol $\text{m}^{-2}\text{d}^{-1}$)

42　in the entire study area from spring to summer. Specifically, the SYS and ECS

43　offshore waters changed from $CO_2$ sinks in spring to sources in summer, while the

44　Changjiang River plume always served as a $CO_2$ sink.

45

46　**Keywords:** Carbon cycle, air-sea $CO_2$ flux, the South Yellow Sea and East China Sea,

47　seasonal variations

48

49　**Plain Language Summary**

50　　　Although the South Yellow Sea (SYS) and East China Sea (ECS) are adjacent to

51　each other, the biogeochemical characteristics of them are very different. Therefore, a

52　study of the SYS and ECS together will allow us a better understanding of the

53　processes determining the spatial and temporal variations of the carbonate system in

54　continental seas, which is an important step toward estimating global air-sea $CO_2$

55　fluxes. In this study, two cruises were conducted in early spring and summer to

56　investigate the distributions of the carbonate system in the SYS and ECS. High

57　dissolved inorganic carbon (DIC) and alkalinity were observed in the SYS under the

58　influence of Yellow River with high DIC and alkalinity discharges. However, low

59　DIC, alkalinity and high pH values occurred in the Zhe-Min Coastal Current. The

60　distribution and variability of the partial pressure of $CO_2$ were associated with

61　temperature, biological activity and physical mixing. Under the combined impacts of

62　the above factors, the SYS and ECS offshore waters changed from $CO_2$ sinks in

63　spring to sources in summer, while the Changjiang River plume always served as a

64  $CO_2$ sink. Overall, Strong $CO_2$ sinks turned into weak sources in this region from

65  spring to summer.

66

67  **1 Introduction**

68      In the last two decades, continental shelves have drawn increasing attention in

69  the global ocean carbon cycle research due to the fact that they provide 15–30% of the

70  oceanic primary production and represent 50% of ocean organic carbon burial in

71  sediments, although shelves just comprising approximately 7% of the world's ocean

72  surface area (Bauer et al., 2013; Borges et al., 2005; Cai, 2011; Chen, 2003). The

73  continental shelves are distinguished by the intense physical, chemical and biological

74  processes, and considered to be significant contributors to the global carbon cycle

75  (Mackenzie et al., 1991). It is therefore necessary to understand and accurately

76  account for the variability of air-sea $CO_2$ flux and carbonate chemistry of continental

77  shelves although it remains a tremendous challenge to make satisfactory progresses

78  (Bauer et al., 2013; Zhai et al., 2014).

79      There are large spatial and temporal variations in surface seawater

80  biogeochemistry and air-sea $CO_2$ exchanges across heterogeneous continental shelves

81  (Takahashi et al., 2009). An ocean margin province-based synthesis by Cai et al.

82  (2006) suggested that continental marginal seas at low latitudes were the major $CO_2$

83  sources (Cai et al., 2003, 2004; Goyet et al., 1998), but those in mid-high latitudes

84  were the sinks of atmospheric $CO_2$ (DeGrandpre et al., 2002; Thomas et al., 2005;

85  Tsunogai et al., 1999). Recently, Dai et al. (2013) suggested that margins receiving

86 river inputs (RiOMar) were largely a $CO_2$ sink while those receiving ocean inputs

87 (OceMar) were largely sources of $CO_2$ to the atmosphere. However, these broad

88 classifications may oversimplify the field observations and the mechanisms leading to

89 these synthesis statements require further supports from many field studies in

90 dissimilar margins. For example, the North Sea, a European continental shelf sea, is a

91 $CO_2$ sink in the northern part but a $CO_2$ source in the southern part under the influence

92 of temperature, terrestrial inputs and biological activity from north to south (Bozec et

93 al., 2005; Kempe & Pegler, 1991; Omar et al., 2010; Thomas et al., 2005). Similarly,

94 the partial pressure of $CO_2$ ($pCO_2$) distribution also shows a different spatial trend in

95 the adjacent South Yellow Sea (SYS) and East China Sea (ECS), resulting from

96 different topography, ocean circulation and biogeochemical conditions. In the north,

97 the SYS, as a semi-enclosed marginal sea, is a net annual $CO_2$ source because of its

98 long water residence time and limited water exchange with open ocean (Qu et al.,

99 2014; Xue et al., 2011; Zhang et al., 2010). In contrast, in the south, the ECS is an

100 eminent continental shelf pump for efficient transferring atmospheric $CO_2$ to the deep

101 sea and serves as an annual net sink of atmospheric $CO_2$ (Song et al., 2018; Tsunogai

102 et al., 1999; Wang et al., 2000; Zhai & Dai, 2009). Therefore, the carbonate

103 characteristics of these two seas are different. However, the previous studies tend to

104 study their air-sea flux separately, even if the SYS and ECS are adjacent to each other.

105 To our best knowledge, the carbonate system of the entire SYS and ECS (together

106 called the South Yellow-East China Sea region) has only been investigated in the

107 spring and summer of 2011 and the summer of 2013 (Qu et al., 2015, 2017) to date.

108   With those limited studies, the spatial resolution of $pCO_2$ distributions is still lacking

109   because the $pCO_2$ in Qu et al. (2015, 2017) was calculated by CO2SYS based on the

110   discrete pH and total alkalinity (TA) instead of continuous underway measurement,

111   and the air-sea $CO_2$ flux based on discrete estimations also had great uncertainties.

112       A better understanding of spatial and temporal variations of carbonate system in

113   the South Yellow-East China Sea region is important to merge its $CO_2$ flux into the

114   global carbon cycle. Therefore, in this study, we investigated high spatial resolutions

115   of discrete pH, dissolved inorganic carbon (DIC) and TA samples as well as

116   underway $pCO_2$ in the South Yellow-East China Sea region with intensive biological

117   activity based on two cruises from 27 March to 11 April, 2017 and 27 June to 17 July,

118   2018. We also calculated the air-sea $CO_2$ fluxes and examined the driver mechanisms

119   to impact the $pCO_2$ variations and air-sea $CO_2$ fluxes. This study fills in the

120   knowledge gap by not only providing an updated dataset on the air-sea $CO_2$ fluxes in

121   the South Yellow-East China Sea region, but also improving our understanding of

122   carbon cycles in continental seas.

123

124   **2 Materials and Methods**

125   **2.1 Study area**

126       The South Yellow and East China Sea, which is located in the northwestern

127   Pacific Ocean between 26–37°N and 119–125°E (Figure 1). The SYS is a

128   semi-enclosed marginal sea, which is surrounded by the Shandong and Korean

129   Peninsulas and bordered on the north by the North Yellow Sea and on the south by the

130   ECS. It is distinguished and dominated by several major water masses in different

131  seasons, including the Yellow Sea Warm Current, Yellow Sea Cold Water Mass,

132  coastal water currents along both the Chinese and Korean coasts and Changjiang

133  River (Figure 1). Moreover, the Subei Shoal waters in the southwestern SYS, being

134  one of the most turbid coasts in China, load numerous sediments into the SYS

135  annually (Wang et al., 2011a). Hence, the SYS is strongly influenced by nearshore

136  biogeochemical processes, intense anthropogenic activities to a great extent and is

137  isolated from open sea (Choi et al., 2019). However, the ECS is located to the south of

138  the SYS and the western three quarters of the ECS is occupied by the continental shelf,

139  while the eastern part is deep and opens to the Pacific Ocean (Chen, 2009). The

140  materials from the Pacific Ocean is easily exchanged with the ECS by the Kuroshio

141  Current (KC) and Taiwan Warm Current (TWC), while the Changjiang River brings

142  large amounts of terrigenous nutrients into the ECS (Qu et al., 2017). Thus, the

143  carbonate system in the ECS is strongly subjected to the continental shelf pump

144  between the nearshore and open sea (Tsunagai et al., 1999). Given these points, the

145  South Yellow-East China Sea region becomes a biogeochemical hotspot all the time

146  due to the large differences in the physical and biogeochemical conditions between

147  the SYS and ECS.

148
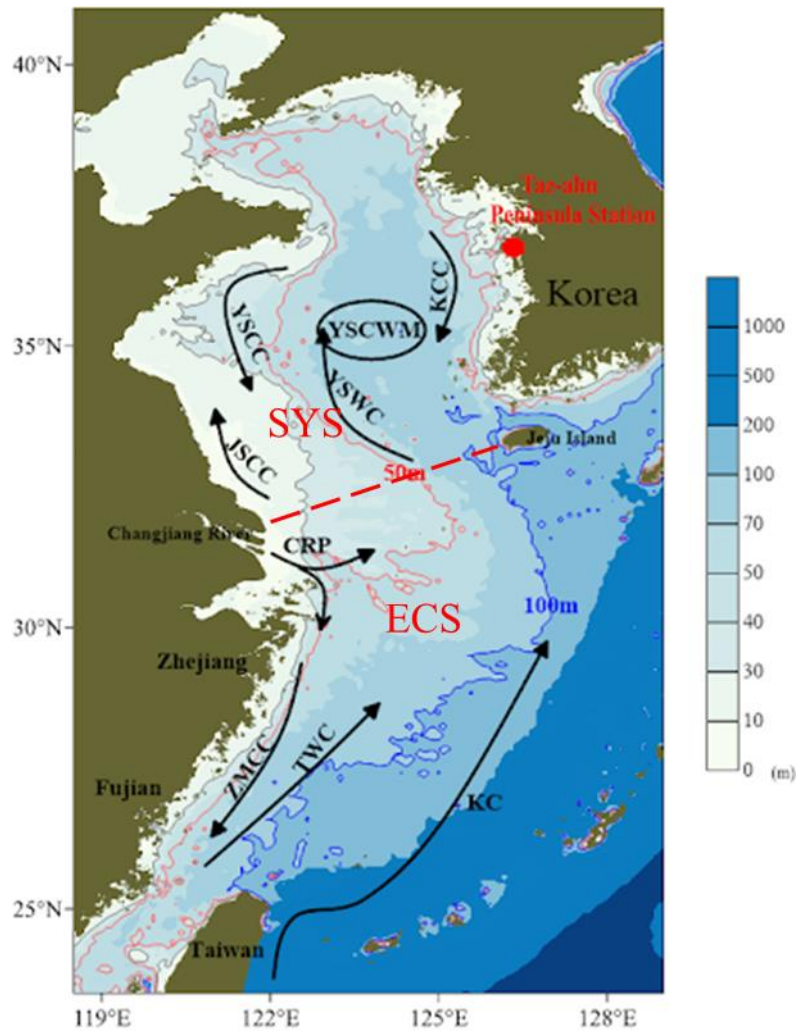
**Figure 1.** Topography and schematic map of the current system in the study area. The

boundary of the South Yellow Sea (SYS) and East China Sea (ECS) is indicated by

the red dashed-line. The currents described as arrows include the Yellow Sea Coastal

Current (YSCC), Yellow Sea Warm Current (YSWC), Yellow Sea Cold Water Mass

(YSCWM), Korea Coastal Current (KCC), Jiangsu Coastal Current (JSCC),

Changjiang River plume (CRP), Zhe-Min Coastal Current (ZMCC), Taiwan Warm

Current (TWC) and Kuroshio Current (KC) (Chen, 2009). The red and blue solid lines

on the continental shelf are the depth contour of 50 and 100 m, respectively. The red

dot (126.133°E, 36.738°N) in the west part of South Korea is the Tae-ahn Peninsula

Station (https://www.esrl.noaa.gov).

159

**2.2 Sampling**

Two cruises were carried out aboard the R/V *"Dongfanghong II"* from 27 March

to 11 April, 2017 and 27 June to 17 July, 2018 to represent the early spring and

summer, respectively. The study area and sampling stations are shown in Figure 2.

164
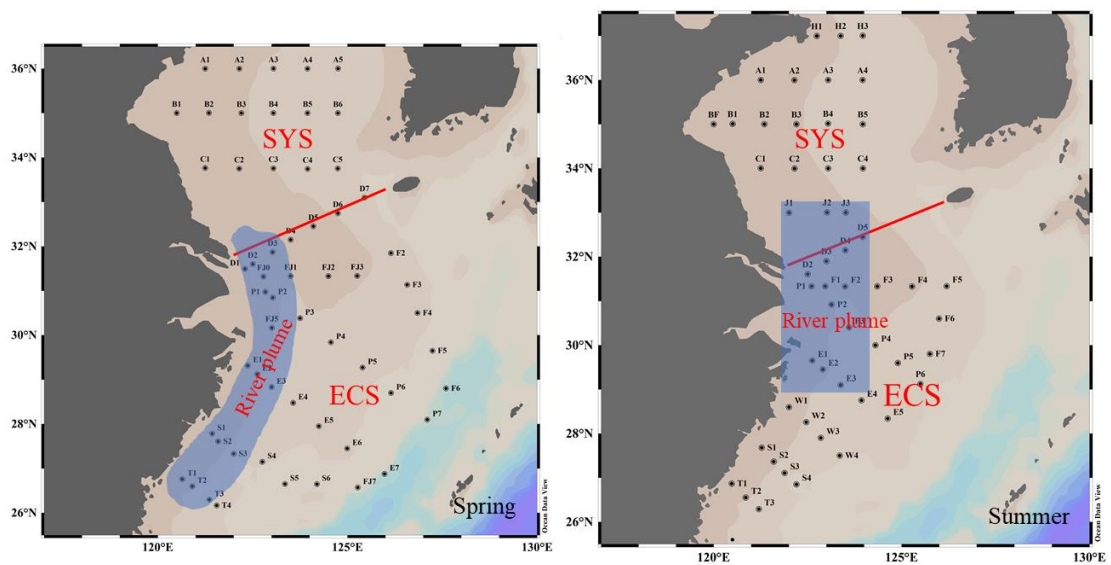


**Figure 2.** Sampling stations of 2017 spring (left) and 2018 summer (right) cruises.

The blue shadows represent the Changjiang River plume; the South Yellow Sea (SYS)

and East China Sea (ECS) are divided by the red solid line.

169

Water samples were collected using 12 L Niskin bottles mounted onto a Seabird

911-plus Conductivity-Temperature-Depth system (CTD, SeaBird Inc. Bellevue, WA,

USA), which was used to measure the temperature and salinity of water column. DO

samples were collected, fixed and analyzed on board as described by the classic

Winkler procedure (Dickson, 1994). pH was collected into a 100 mL narrow-mouth

175  glass bottle and kept in a thermal bath (25 ± 0.1 °C) for 30–60 min before

176  determination. DIC and TA samples were stored in 250 mL borosilicate glass bottles

177  and overflowed at least twice their volume to minimize contact with air, then

178  poisoned with 100 μL of saturated $HgCl_2$ immediately, sealed and preserved at room

179  temperature until determination (Huang et al., 2012). 300 mL water samples were

180  filtered through a 0.7 μm-pore Whatman glass fiber filter (GF/F, pre-combusted at

181  400 °C for 4 h), and materials collected on the membrane were preserved at -20 °C

182  and used for analyzing Chlorophyll *a* (Chl *a*).

183  To monitor levels of $p$$CO_2$, surface water was continuously pumped from 1–2 m

184  below the sea level through an underway $p$$CO_2$ analyzer (AS-P2, Apollo SciTech Inc.,

185  USA) with a Picarro detector (G2301, Picarro Inc., USA) installed in the shipboard

186  laboratory. Briefly, surface water was pumped to the main shower-head equilibrator at

187  a rate of 2.5 L $min^{-1}$ to get rapid gas exchange. After the sample was equilibrated, the

188  well-mixed gas first passed through the water condenser and desiccant, which

189  removed most of the water vapor, and then the equilibrated gas was delivered to the

190  detector (Picarro G2301). The detector was calibrated every 9 h against three $CO_2$ gas

191  standards (0, 198 and 403 ppm), which were provided by Beijing Certified Reference

192  Material Center. Some values of $x$$CO_2$ outside of the concentration range of the

193  standard gases were also used in this study because the biases caused by the

194  out-of-range values are generally subtle (Pierrot et al., 2009). The uncertainty of $x$$CO_2$

195  measurements was less than 50 ppbv over 5 min internals (Li et al., 2017).

196

## 2.3 Analytical methods

pH was measured onboard at 25 ± 0.1 °C by Fisher pH meter (Star A211) combining with a Ross Orion combination electrode (Ross-8102) on a National Bureau of Standards (NBS) scale with a precision of ± 0.01 units. pH values were corrected to the in-situ temperature using CO2SYS. 1 mL of each DIC sample was acidified by 10% phosphoric acid, then the extracted $CO_2$ gas with carrier gas was quantified via an infrared gas analyzer (AS-C3, Apollo SciTech Inc., USA) as described in Cai et al. (2004). TA samples were determined by Gran titration on a 25 mL sample volume using the open-cell method with a semi-automatic potentiometric titration system (AS-ALK2, Apollo SciTech Inc., USA) (Cai et al., 2010). Both DIC and TA measurements were calibrated against certified reference materials from A. G. Dickson's lab at Scripps Institute of Oceanography (Batches #162 and #171) at a precision of ± 2 μmol $kg^{-1}$ (Huang et al., 2012).

Chl *a* on the membrane was extracted in 90% acetone and then analyzed by a fluorescence spectrophotometer (F-4500, Hitachi, Japan) based on the procedure described by Parsons et al. (1984).

## 2.4 Air-sea $CO_2$ flux estimation

In this study, the $pCO_2$ at the temperature of equilibration ($pCO_2(eq)$, unit: μatm) in equation (1) is calculated as following and then the $pCO_2$ at the in-situ temperature ($pCO_2(water)$, unit: μatm) in equation (2) is calculated by the expression of Takahashi et al. (1993):

219       $pCO_2(eq) = xCO_2 \times [P_b(eq) - P_w(eq)]$                   (1)

220       $pCO_2(water) = pCO_2(eq) \times \exp[0.0423 \times (SST - T_{eq})]$          (2)

221       where $xCO_2$ is the $CO_2$ mole fraction concentration of the seawater $CO_2$ in the dried

222       sample gas flow (ppm), $P_b(eq)$ is the barometric pressure of equilibration and $P_w(eq)$

223       is the water vapor pressure at 100% humidity calculated by the equilibrated

224       temperature ($T_{eq}$, °C) and in-situ salinity (Weiss & Price, 1980). $SST$ (°C) is the in-situ

225       temperature of surface water, the temperature difference between the in-situ water and

226       the equilibration was less than 0.5 °C.

227            The air-sea $CO_2$ fluxes ($FCO_2$, mmol m$^{-2}$ d$^{-1}$) were estimated as follows:

228       $FCO_2 = 0.24 \times k \times K_H \times [pCO_2(water) - pCO_2(air)]$            (3)

229       where $k$ (cm h$^{-1}$) is the gas transfer velocity of $CO_2$, $K_H$ (mol L$^{-1}$ atm$^{-1}$) is the

230       solubility constant of $CO_2$, calculated from in-situ temperature and salinity (Weiss,

231       1974), and $pCO_2(water)$ and $pCO_2(air)$ are the $pCO_2$ in the surface seawater and the

232       atmosphere, respectively. The atmospheric $pCO_2$ values (417 µatm in April 2017 and

233       398 µatm in July 2018) were estimated from the monthly atmospheric $xCO_2$ (418.49

234       ppm in April 2017 and 410.14 ppm in July 2018) at Tae-ahn Peninsula (126.133°E,

235       36.738°N, Figure1) (https://www.esrl.noaa.gov), after correction for water vapor

236       pressure at 100% humidity with in-situ temperature and salinity data  (Weiss and

237       Price, 1980). A positive flux value represents a release of $CO_2$ from the water body to

238       the atmosphere, while a negative value indicates $CO_2$ transfer from the atmosphere to

239       the water body. The gas transfer coefficient was calculated from wind speed based on

240       the Wanninkhof (2014) empirical function:

241     $k$ (cm h$^{-1}$) = 0.251 × $U^2$ × ($Sc$/660) $^{-0.5}$                    (4)

242     where $U$ (m s$^{-1}$) is the wind speed at 10 m above the water surface, the reanalyzed

243     monthly averaged wind speed (5.95 and 6.00 m s$^{-1}$ in spring and summer, respectively)

244     provided by the European Center for Medium-Range Weather Forecasts (ECMWF)

245     was employed to calculate the air-sea $CO_2$ fluxes; $Sc$ is the Schmidt number of $CO_2$ in

246     seawater; 660 is the $Sc$ value in seawater at 20 °C.

247

248     **3 Results**

249     **3.1 Hydrographic conditions**

250           Surface seawater temperature (SST) presented significant temporal and spatial

251     variations (Figure 3). SST was in the range of 6.91–24.47 and 15.82–28.17 °C, with

252     average (± SD) values of 14.00 ± 5.00 and 24.94 ± 2.80 °C, respectively, in the spring

253     and summer throughout the South Yellow-East China Sea region. clearly SST

254     increased homogeneously with the decreasing latitudes in spring and summer. On

255     average, SST in the SYS was 7.31 and 4.94 °C colder than that in the ECS in early

256     April and July, respectively. The temperature difference between the SYS and ECS in

257     April was due to the increase of atmospheric temperature from north to south in the

258     northern hemisphere, while in July, it could be mainly attributed to the intrusion of the

259     TWC or KC with the influence of the summer monsoon (Chen, 2009). The ranges of

260     salinity in spring (range: 25.81–34.94, average: 32.59 ± 1.89) and summer

261     (23.63–34.14, average: 31.58 ± 2.26) were not greatly different. The main feature was

262     that a water tongue with relatively low salinity rushed out of Changjiang estuary and

263  formed a plume, indicating the influence of the Changjiang River on the junction of

264  the SYS and ECS. This plume feature was stronger in summer than spring.

265
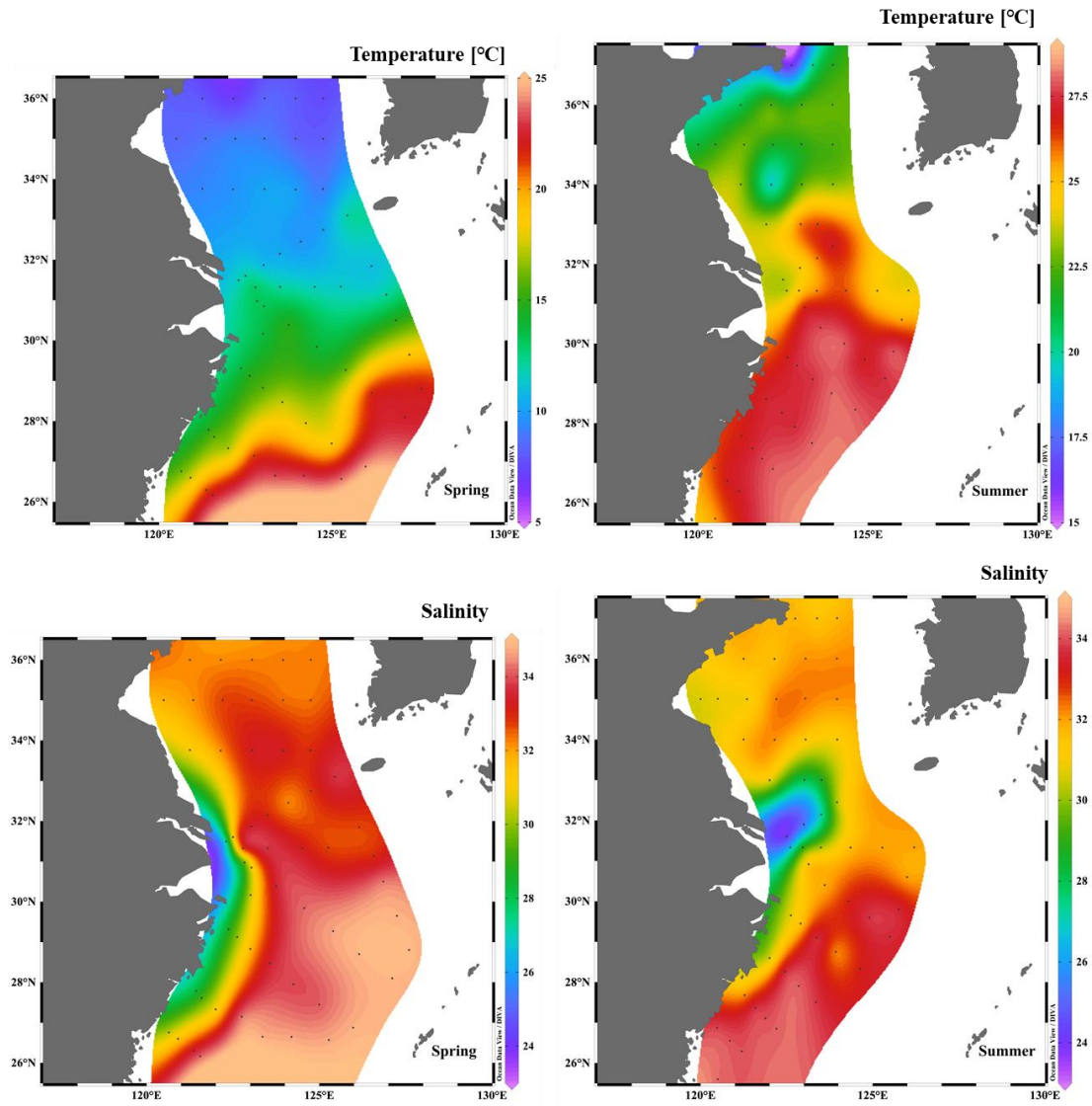


267  **Figure 3.** Horizontal distributions of temperature (°C) and salinity in the surface

268  water of spring and summer.

269

270  From early spring to summer, the surface Chl *a* exhibited considerable variation

271  (Figure 4). Overall, Chl *a* concentration of the SYS in early spring ($0.59 \pm 0.51$ μg L$^{-1}$)

272    was lower than that (1.00 ± 0.98 µg L$^{-1}$) in summer because of the weak biological

273    activity at lower temperature. In summer, high Chl *a* value appeared in the

274    southwestern part of the SYS, which was enhanced by the abundant nutrient inputs

275    from the Changjiang River. In the ECS, high concentrations of surface Chl *a*

276    (3.46–8.80 µg L$^{-1}$) in spring were found in the southwest part of the shelf near the

277    coast. Also noted was high Chl *a* concentration in the northwest part of the ECS in

278    summer, which was also due to the large amount of nutrients loading from the

279    Changjiang River. In contrast, low surface Chl *a* (< 0.50 µg L$^{-1}$) was observed in the

280    middle and outer shelves of the ECS in both spring and summer.

281        $O_2$ saturation in surface water were oversaturated conditions albeit with a few

282    exceptions (Figure 4). The average $O_2$ saturations were 109 ± 13 and 152 ± 17% in

283    the surface layer of the South Yellow-East China Sea region during spring and

284    summer cruises, respectively. Thus, $O_2$ saturation in the surface layer of summer was

285    higher than that in spring, due to the growth of phytoplankton and water stratification,

286    which limited the exchanges between high DO in the surface layer and low DO in the

287    bottom layer.

288
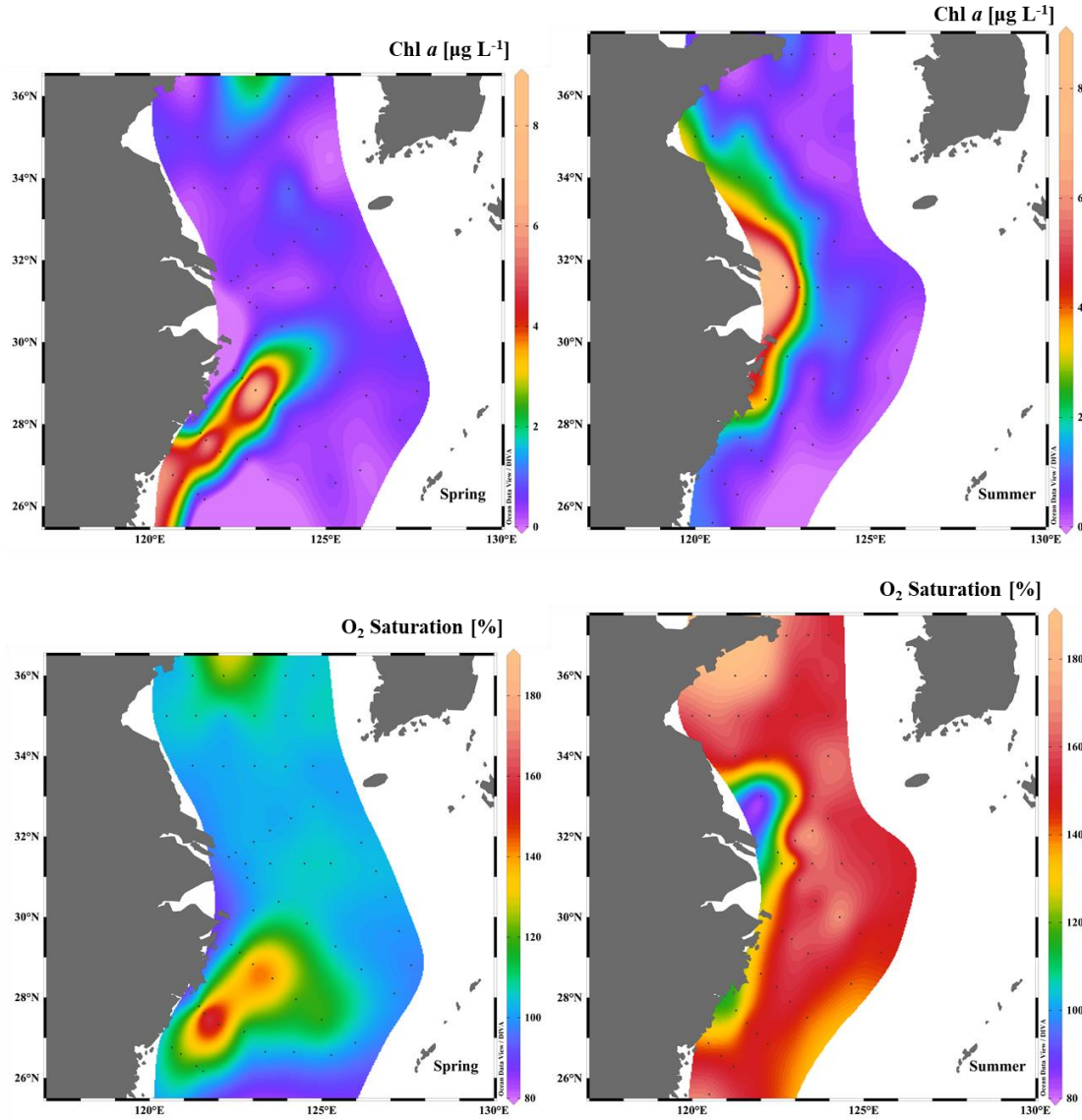
**Figure 4.** Horizontal distributions of Chl $a$ ($\mu g$ $L^{-1}$) and $O_2$ saturation (%) in the surface water of spring and summer.

**3.2 Distributions of carbonate system parameters**

Surface pH of the South Yellow-East China Sea region from 8.06 to 8.50, and 8.02 to 8.54 in spring and summer, with the averages of $8.20 \pm 0.09$ and $8.19 \pm 0.09$, respectively. Overall, pH increased from north to south, and the highest pH values (8.31–8.50) were mainly located in the southwestern part of the ECS. In summer, the

298    isoline of pH was basically perpendicular to the shoreline and the low pH appeared in

299    the coastal waters, whereas the high values of pH (8.27–8.54) were mainly observed

300    in the river plume region (Figure 5).

301        Surface DIC values were in the range of 1868 to 2089 and 1826 to 2159 μmol

302    $kg^{-1}$, averaging $1997 \pm 54$ and $1982 \pm 82$ μmol $kg^{-1}$ in spring and summer, respectively.

303    The surface DIC concentration exhibited both spatial variations and clear seasonal

304    patterns in different subregions: a slight decreasing in the whole ECS region and an

305    increasing trend in the SYS region from spring to summer. surface TA values were

306    observed in the range of 2113–2318 and 2146–2410 μmol $kg^{-1}$ in spring and summer,

307    respectively, averaging $2244 \pm 47$ and $2264 \pm 50$ μmol $kg^{-1}$. In early spring, TA was

308    homogenous in the central SYS, the middle and outer shelves of the ECS. A few

309    higher values ($2306 \pm 9$ μmol $kg^{-1}$) existed in the coastal waters of the SYS while

310    lower values ($2154 \pm 29$ μmol $kg^{-1}$) appeared in the southwestern ECS. On the other

311    hand, TA in summer decreased from north to south in the SYS and fluctuated with a

312    narrow range in the ECS ($2247 \pm 17$ μmol $kg^{-1}$). However, the distribution of

313    normalized TA (TA/S) decreased with the increasing salinity, which was greatly

314    different from TA distribution (Figure 5).

315
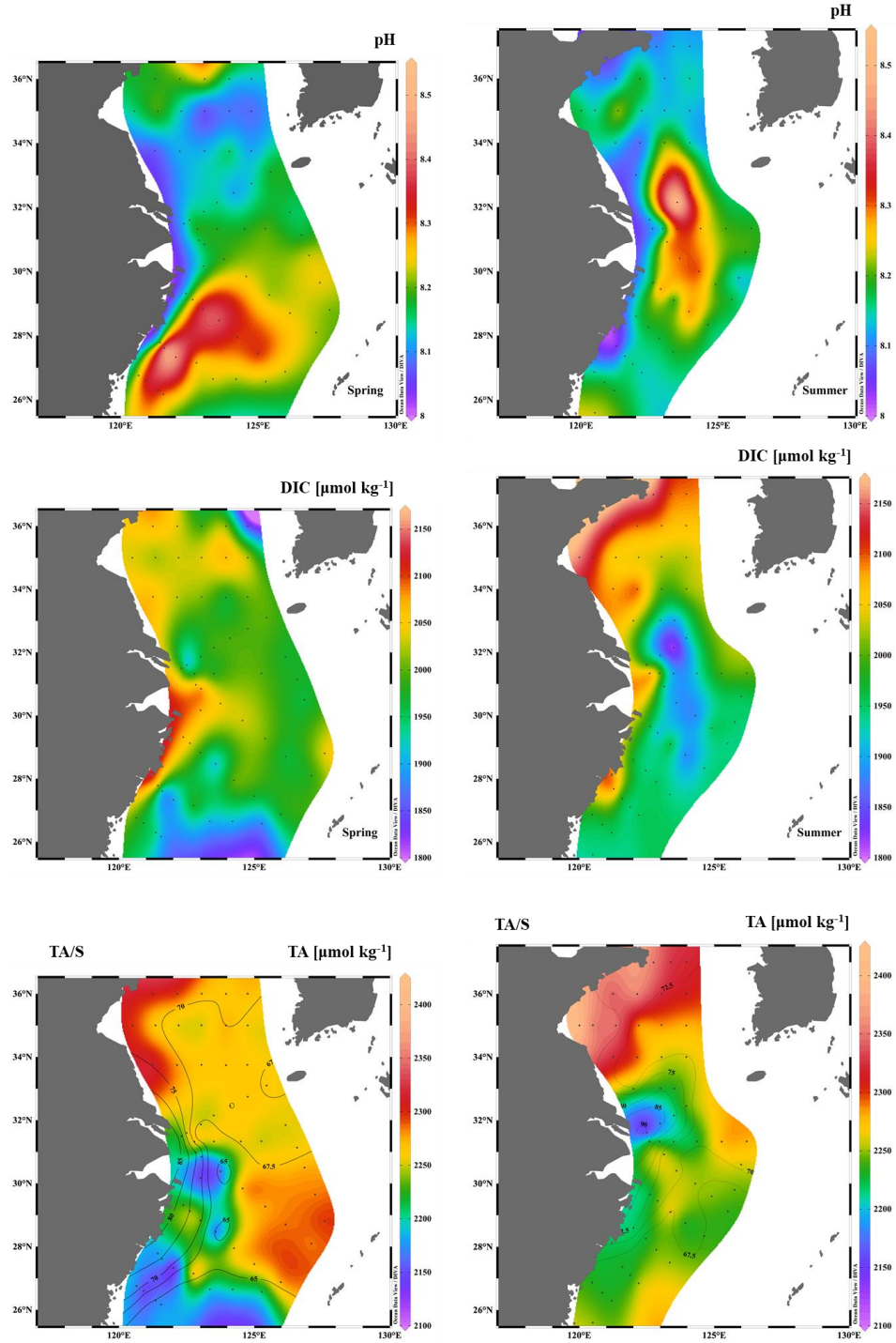
**Figure 5.** Horizontal distributions of pH, DIC (μmol kg$^{-1}$) and TA (μmol kg$^{-1}$) in the surface water during spring and summer. The coutour in the lower pannel represent the distribution of TA/S.

The underway $p$CO$_2$ data during the two cruises allow us to examine the

322 high-resolution distribution of $pCO_2$ in the South Yellow-East China Sea region

323 (Figure 6). During our sampling period, even though $pCO_2$ values showed similar

324 ranges between early spring (151–689 µatm) and summer (149–709 µatm), the

325 averaged $pCO_2$ values were significantly higher in summer (409 ± 71 µatm) than

326 those in spring (360 ± 75 µatm). In spring, supersaturated $pCO_2$ values were observed

327 near the Subei shoal waters (447–611 µatm), whereas $pCO_2$ values in the rest of SYS

328 were generally low (258–407 µatm), except that $pCO_2$ in the central SYS (420–444

329 µatm), which was a little higher than the atmospheric $pCO_2$. However, in summer,

330 $pCO_2$ in the SYS was generally high (>420 µatm) except that in the southern SYS,

331 resulting from Changjiang diluted water input. In addition, few sporadic low $pCO_2$

332 values were found near the south of the Shandong Peninsula. In the river plume, $pCO_2$

333 in spring kept in a low range (<355 µatm) except in the area near the Changjiang

334 mouth and the northwestern corner (513–689 µatm), as well as in Hangzhou Bay

335 (421–455 µatm). To the contrary, Changjiang estuary mouth and the northwestern

336 corner showed relatively low $pCO_2$ (149–386 µatm) in summer, however, high $pCO_2$

337 in the range of 420–470 µatm occurred in the coastal water near the Hangzhou Bay.

338 The seasonal patterns in the northern and southern of ECS offshore water were

339 different: $pCO_2$ in the northern ECS always showed relatively low $pCO_2$ in spring and

340 summer; while southern ECS had low $pCO_2$ (<380 µatm) in spring and high $pCO_2$ in

341 summer (>430 µatm).

342      Similar to the seasonality of $pCO_2$ in the South Yellow-East China Sea region,

343 the air-sea $CO_2$ fluxes also had strong seasonal variations in the range of -18.63–19.46

344    and -18.03–22.61 mmol m$^{-2}$ d$^{-1}$, with the average values of -4.11 ± 5.28 and 0.88 ±

345    5.09 mmol m$^{-2}$ d$^{-1}$ in spring and summer, respectively (Figure 6). The SYS and ECS

346    were significant atmospheric $CO_2$ sinks in spring, with average values of -2.11 ± 4.57

347    and -5.56 ± 3.12 mmol m$^{-2}$ d$^{-1}$, but shifted into $CO_2$ sources (2.35 ± 4.30 and 1.73 ±

348    3.05 mmol m$^{-2}$ d$^{-1}$) in summer. However, the river plume always acted as a strong

349    $CO_2$ sink in both spring and summer (-3.78 ± 7.44 and -5.17 ± 6.65 mmol m$^{-2}$ d$^{-1}$). In

350    addition, the Subei shoal waters was always a $CO_2$ source during these two surveys.

351



352
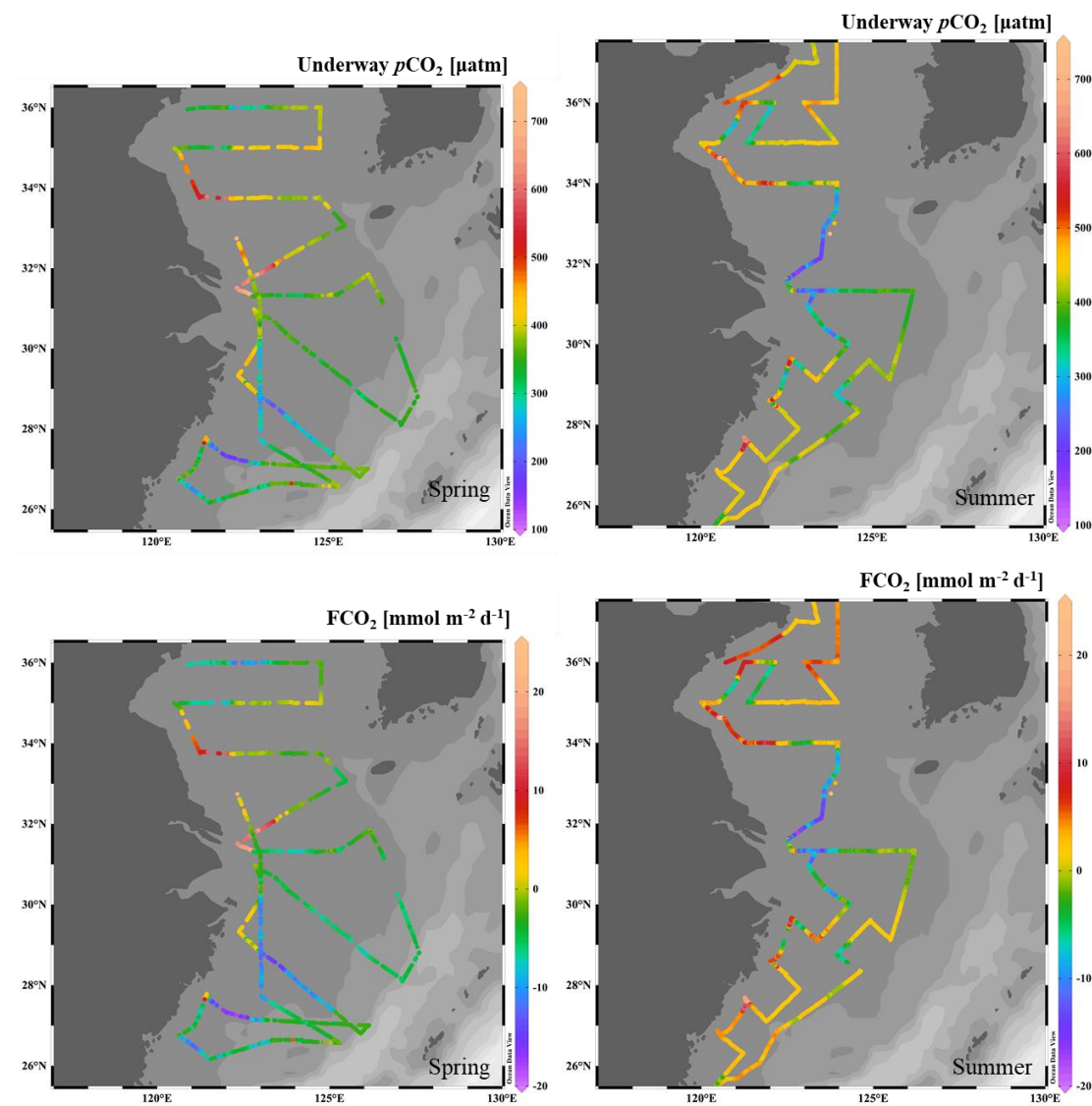
353     **Figure 6.** The trajectory of underway $pCO_2$ (μatm) and air-sea $CO_2$ flux (mmol m$^{-2}$

354     d$^{-1}$) in the surface water during spring and summer.

355

356     **4 Discussion**

357     **4.1 Classification of the water mass types**

358         In order to understand the biogeochemistry of the South Yellow-East China Sea

359     region and explore the influencing mechanism of carbonate system, it is necessary to

360     describe typical water mass distributions in this study. On the basis of the

361     temperature-salinity characteristics (Figure 7), surface waters were divided into three

362     subregions: (1) SYS, (2) River plume and (3) ECS offshore waters. The ranges of the

363     hydrological and carbonate system parameters in these three subregions are

364     summarized in Table 1, and the areal distributions of these water masses are presented

365     in Figure 2. The SYS has low temperature and moderate salinity; the ECS offshore

366     waters are mainly impacted by the KC and TWC (Chen, 2009). The KC flows

367     northeast along the shelf break and TWC enters the ECS through Taiwan Strait and

368     traverses in the middle shelf (Lee & Chao, 2003). Both KC and TWC are

369     characterized by high salinity and temperature (Chou et al., 2009). It is worth noting

370     that the location of river plume varied from April to July under the influence of

371     seasonal monsoons (Qi et al., 2014), which was further illustrated by the distribution

372     of salinity (Figure 3). For example, the low salinity in the river plume was roughly

373     confined to the nearshore from 26 to 32 °N in spring because the influence of the

374     prevailing northeast wind (Wu et al., 2014). When it comes to summer, the

375    Changjiang River, carrying the nutrients, rushed out towards its northeast and formed

376    river plume, triggering the high primary productivity there (Isobe & Matsuno, 2008).

377



378
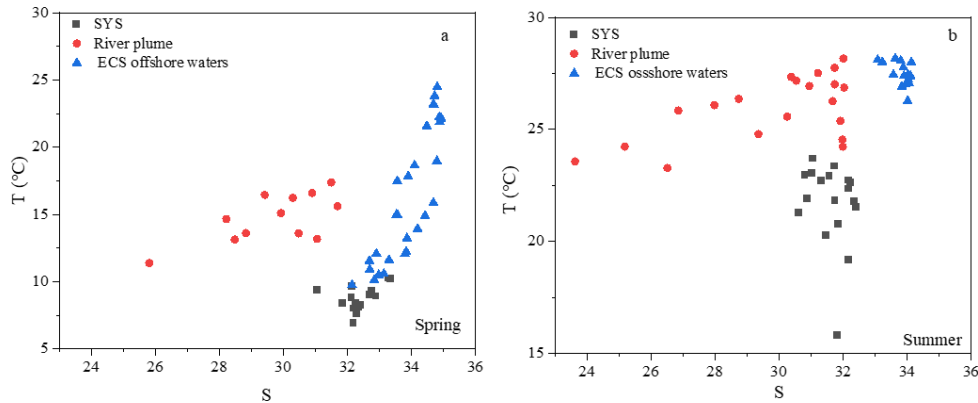
379    **Figure 7.** Temperature (T) vs. salinity (S) in surface water of the South Yellow-East

380    China Sea region during spring (a) and summer (b) for three water masses: SYS, river

381    plume and ECS offshore waters.

382

383    **Table 1.** Hydrological and carbonate parameters of the different water masses in the

384    surface layer defined in this study.

385

| Subregion | Longitude (°E) | Latitude (°N) | T (°C) | S | Chl $a$ ($\mu$g L$^{-1}$) | DO Saturation (%) |
|---|---|---|---|---|---|---|
| *Spring* SYS | 120.0–125.5 | 33.0–36.0 | 6.91–10.25 | 31.05–33.36 | 0.07–1.93 | 101–125 |
| | | | (8.71 ± 0.91) | (32.39 ± 0.55) | (0.59 ± 0.51) | (106 ± 6) |
| River plume | 122.0–123.5 | 28.0–32.0 | 11.37–17.38 | 25.81–32.26 | 0.23–8.80 | 100–167 |
| | 120.0–122.0 | 26.0–28.0 | (14.55 ± 1.85) | (29.92 ± 1.76) | (2.66 ± 2.97) | (117 ± 22) |

| Subregion | | | | | | |
|---|---|---|---|---|---|---|
| ECS offshore | 123.5–127.6 | 28.0–33.0 | 9.75–24.47 | 32.15–34.94 | 0.03–1.88 | 98–141 |
| | 122.0–126.2 | 25.5-28.8 | (16.47 ± 5.01) | (33.90 ± 0.82) | (0.49 ± 0.41) | (106 ± 9) |
| *Summer* SYS | 120.0–125.5 | 33.0–37.5 | 15.82–23.70 | 30.61–32.40 | 0.16–3.03 | 82–188 |
| | | | (21.71 ± 1.87) | (31.64 ± 0.57) | (1.00 ± 0. 98) | (156 ± 21) |
| River plume | 122.0–124.3 | 29.0–33.0 | 23.28–27.76 | 23.63–31.74 | 0.57–8.22 | 122–173 |
| | | | (25.98 ± 1.43) | (29.12 ± 2.56) | (2.74 ± 2.41 | (150 ± 18) |
| ECS offshore | 124.3–126.2 | 29.0–33.0 | 24.23–28.17 | 31.93–34.14 | 0.13–1.21 | 120–174 |
| | 120.0–125.5 | 25.5–29.0 | (27.08 ± 1.15) | (33.37 ± 0.86) | (0.52 ± 0.36) | (149 ± 10) |

386

387 (Table 1 continued)

| Subregion | pH | DIC ($\mu mol\ kg^{-1}$) | TA ($\mu mol\ kg^{-1}$) | Underway $pCO_2$ ($\mu atm$) | $FCO_2$ ($mmol\ m^{-2}\ d^{-1}$) |
|---|---|---|---|---|---|
| *Spring* SYS | 8.06–8.24 | 1965–2071 | 2251–2318 | 258–611 | -12.44–14.08 |
| | (8.14 ± 0.05) | (2028 ± 30) | (2275 ± 20) | (393 ± 61) | (-2.11 ± 4.57) |
| River plume | 8.11–8.50 | 1868–2089 | 2113–2259 | 170–689 | -17.48–19.46 |
| | (8.24 ± 0.13) | (2001 ± 78) | (2195 ± 47) | (365 ± 104) | (-3.78 ± 7.44) |
| ECS offshore | 8.11–8.39 | 1877–2046 | 2160–2297 | 151–411 | -18.62–-0.68 |
| | (8.22 ± 0.06) | (1976 ± 41) | (2250 ± 39) | (336 ± 44) | (-5.56 ± 3.12) |
| *Summer* SYS | 8.08–8.36 | 1997–2159 | 2245–2410 | 261–709 | -9.79–22.61 |
| | (8.16 ± 0.07) | (2078 ± 47) | (2316 ±43) | (432 ± 60) | (2.35 ± 4.30) |
| River plume | 8.10–8.54 | 1826–1967 | 2146–2259 | 149–564 | -18.03–11.99 |
| | (8.26 ± 0.12) | (1905 ± 34) | (2224 ± 28) | (326 ± 92) | (-5.17 ± 6.65) |
| ECS offshore | 8.02–8.31 | 1879–2004 | 2223–2280 | 296–664 | -7.11–19.02 |
| | (8.18 ± 0.06) | (1954 ± 26) | (2247 ± 17) | (420 ± 44) | (1.73 ±3.05) |

388

389 **4.2 The carbonate parameters variability in subregions**

390    Two opposite trends can be obtained from the TA-S and DIC-S scatter plots

391    (Figure 8): one with a negative relationship encompassing the data from the SYS and

392    the other with a positive relationship including the river plume samples. Both

393    regressions converge towards the ECS offshore waters and represent the mixing of

394    these three water masses. The corresponding water mass with high TA and DIC

395    originated from the SYS which could be attributed to the very high TA and DIC

396    discharges of the Yellow River, which has intensive carbonate weathering and erosion

397    in the drainage basin (Liu et al., 2014; Zhang et al., 1990). The positive relationship

398    was characterized by the mixing between the Changjiang River and ECS offshore

399    waters. However, DIC near the Hangzhou Bay was little high in spring ((>2000 μmol

400    kg$^{-1}$, shaded grey in Figure 8a), because the DIC-enrich TWC bottom water flowed

401    northward and extended to around 30°N (Li et al., 2012), then mixed well with the

402    surface water in the water column, leading to the high DIC in spring.

403    DIC and TA concentrations in spring were low near the Zhe-Min Coastal Current

404    (Yellow shaded circles in Figures 8a and 8c). It could be related to the river inputs

405    with low DIC and TA values, such as Minjiang River with low DIC concentration of

406    about 500 μmol L$^{-1}$ in April (Qian et al., 2019). Moreover, the high TA/S values

407    (Figure 5) with the low salinity (Figure 3) in the coastal waters also indicated the

408    influences of terrestrial inputs on DIC and TA values (Jiang et al., 2014). On the other

409    hand, the nutrient enrichment phenomenon was observed in the Zhe-Min Coastal

410    Current, which was caused by river runoff and coastal upwelling, enhancing the

411    primary production and lowering DIC values in this area (Wang & Wang, 2007).

412



413
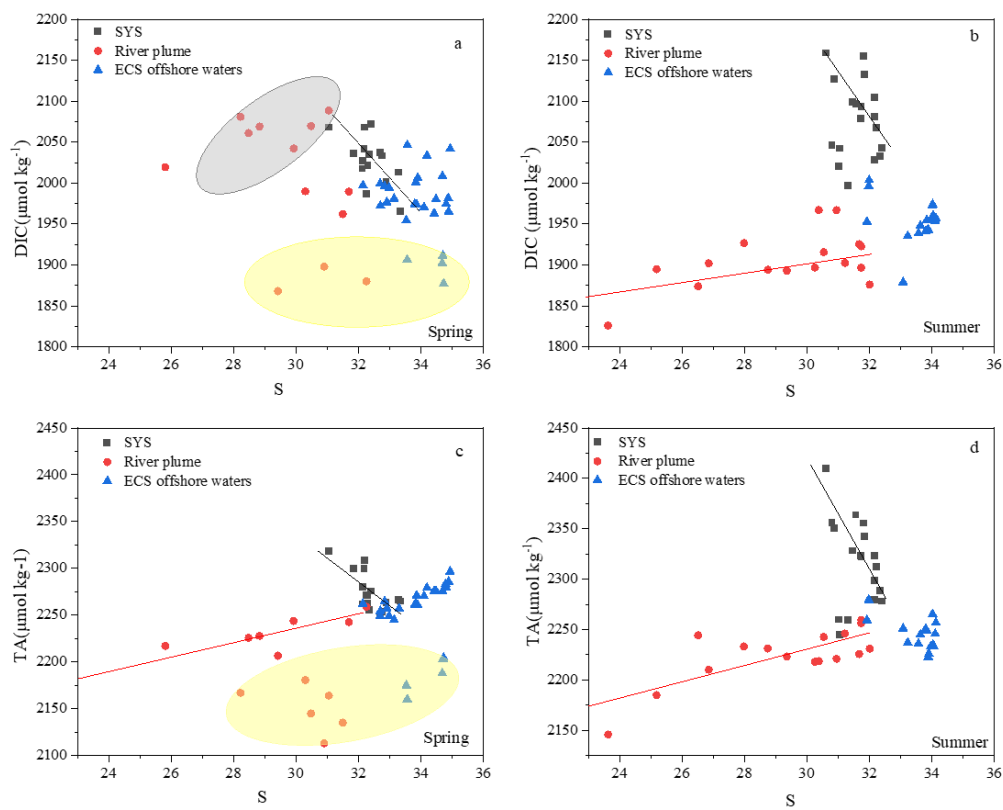
**Figure 8.** The relationships between surface DIC vs salinity (upper panel) and TA vs

salinity (lower panel) in spring and summer in three water masses. The grey shaded

circle represents the stations near the Hangzhou Bay and the yellow shaded circles

represent the stations in the Zhe-Min Coastal Current.

418

### 4.3 Temperature and non-temperature effects on $p$CO$_2$ variability

Field investigations conducted in the global oceans indicate that temperature is

one of the most important factors controlling seawater CO$_2$ (Millero, 1995; Takahashi

et al., 2002) as a consequence of the dependence of the solubility of CO$_2$ with the

temperature (Weiss, 1974). Meanwhile, field observations in the productive

continental shelf seas have demonstrated that biological activity also plays a key role

425  in carbonate characteristics of ocean systems (Takahashi et al., 2002; Thomas et al.,

426  2005; Zhai et al., 2014). In order to quantify the relative importance of temperature

427  and biological effects on the seasonal changes of $pCO_2$ from spring to summer, we

428  calculated the temperature effect in all three subregions with the method proposed by

429  Takahashi et al. (2002). Briefly, the temperature effect can be removed by normalizing

430  $pCO_2$ data at each station to an average temperature (19.31°C) for spring and summer

431  seasons:

432  $pCO_2$ at $T_{mean} = pCO_{2, obs} * \exp [0.0423 (T_{mean} - T_{obs})]$,                    (5)

433  where T is the temperature in °C, and the subscripts "mean" and "obs" indicate the

434  average and observed values, respectively. Thus, the biological activity effect on

435  $pCO_2$ in different subregions described above are discussed based on the relationship

436  between normalized $pCO_2$ ($npCO_2$, normalized to average temperature in this study

437  based on the equation (5)) and Chl $a$ in each station.

438      In the SYS, the different trends between underway $pCO_2$ and SST in spring and

439  summer were found (Figure 9a): a positive correlation ($r = 0.32$, $p < 0.001$) in the

440  middle and north parts (north of the transect C) in April, and negative correlations in

441  the southern part (south of the transect C) in April ($r = -0.72$, $p < 0.001$) and in

442  summer ($r = -0.46$, $p < 0.001$). The positive correlation in the north and middle parts

443  in spring indicated that temperature was the leading role in the $pCO_2$ distribution,

444  which was also found by Liu et al. (2008) in late March and May. Underway $pCO_2$

445  decreased from the west to east along the transect C (Figure 6), which was consistent

446  with the results of high $pCO_2$ in the southwestern SYS (Qu et al., 2017) and low $pCO_2$

447 in the southeastern part (Choi et al., 2019). It is due to the fact that the southwest SYS

448 was occupied by the Subei shoal waters with extremely high concentration of

449 suspended sediment (Wang et al., 2011a) while high biological activity in the

450 southeast SYS (Choi et al., 2019). The negative correlation in July suggested that

451 temperature was no longer the primary factor in controlling the $p$CO$_2$ variability, it

452 tended to be ascribed to the biological activity in this study area (Qu et al., 2014;

453 Zhang et al., 2010). The low $p$CO$_2$ in the southern part was mainly affected by the

454 Changjiang diluted water, which could be seen from the positive correlation between

455 $p$CO$_2$ and salinity in summer (Figure 9b). Similar negative relationships of $p$CO$_2$ and

456 temperature were also reported in the SYS in summer by Qu et al. (2014) and Zhang

457 et al. (2010) and the inner and middle shelves of the ECS in winter (Chou et al., 2011).

458 Therefore, the controlling mechanisms on $p$CO$_2$ variation in the SYS varied with

459 different seasons.

460
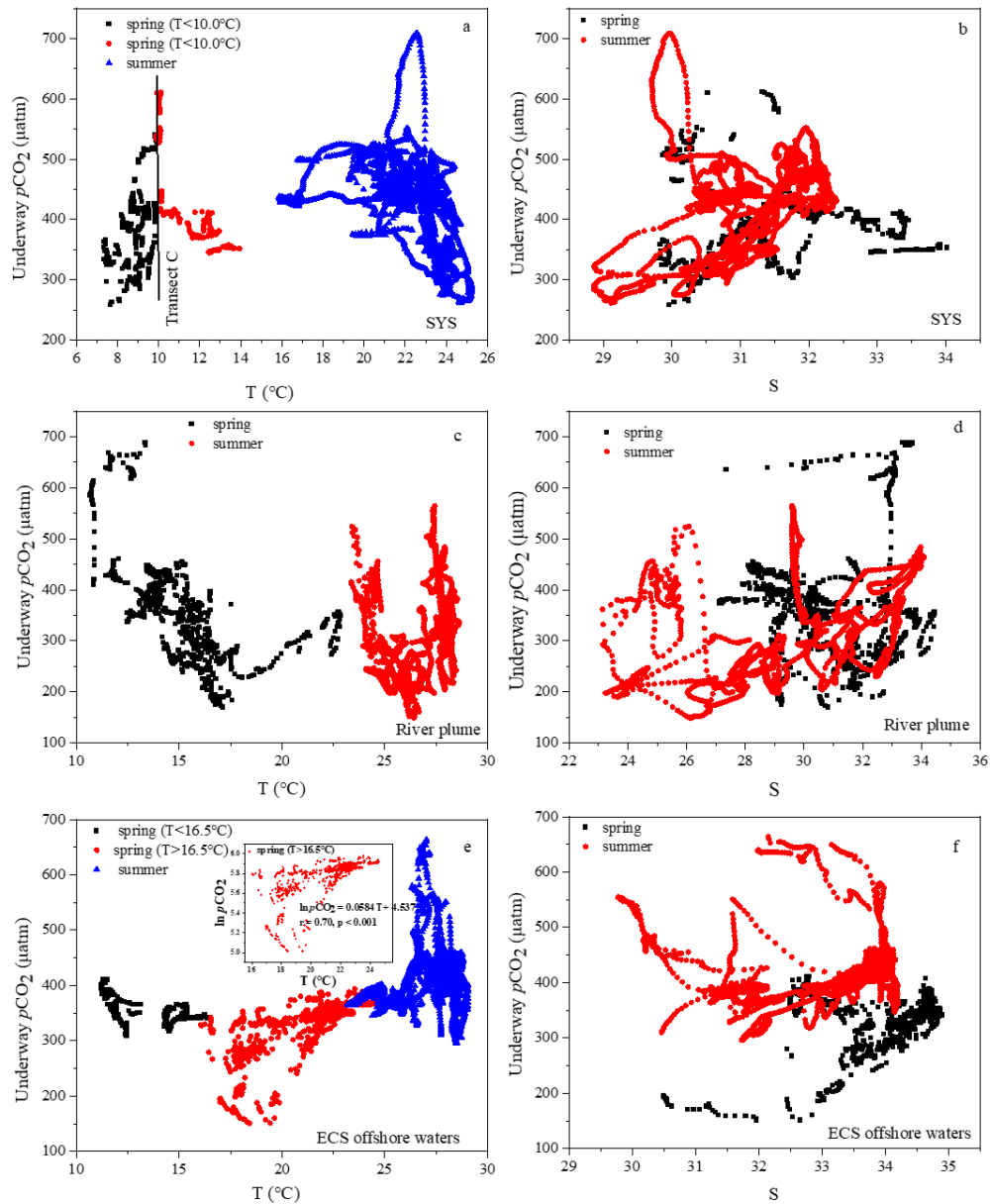
**Figure 9.** Relationships among underway $p$CO$_2$, temperature and salinity in three

subregions in spring and summer. The insert graph in panel (e) shows the relationship

between ln $p$CO$_2$ and temperature when temperature is higher than 16.5°C in the ECS

offshore waters ($\partial\,p$CO$_2\,/\,\partial\,$T $= 0.0584$ °C$^{-1}$).

The negative relationship between n$p$CO$_2$ and Chl $a$ in spring ($r = -0.59$, n $= 14$,

$p < 0.05$) and no conspicuous relationship between them in the SYS during summer

469   (Figure 10a) demonstrated that the effect of biological production on $CO_2$

470   sequestration processes varied with seasons, which was also found by the observation

471   of Qu et al. (2017) in spring and summer of the SYS, 2011. Noted that a weak $CO_2$

472   source replaced a significant $CO_2$ sink in the central SYS in spring (Figure 6), which

473   was opposed to the results of Qu et al. (2014). The reason could be attributed to the

474   fact that a strong vertical mixing still existed in the late-March, and a little bit high

475   $pCO_2$ in the central SYS thus was caused by the upwelling of $CO_2$-riched Yellow Sea

476   Warm Current, which was characterized by high-temperature saline water (Figure S1,

477   see the supplement). Moreover, the onset of the spring phytoplankton bloom in the

478   central SYS usually started from April (Jin et al., 2013; Liu et al., 2015). Therefore,

479   low biological uptake in the central SYS was not strong enough to offset the enhanced

480   $pCO_2$ from the upwelling of the $CO_2$-enriched bottom water. The net result was

481   elevated $pCO_2$ value in the central SYS in early spring.

482
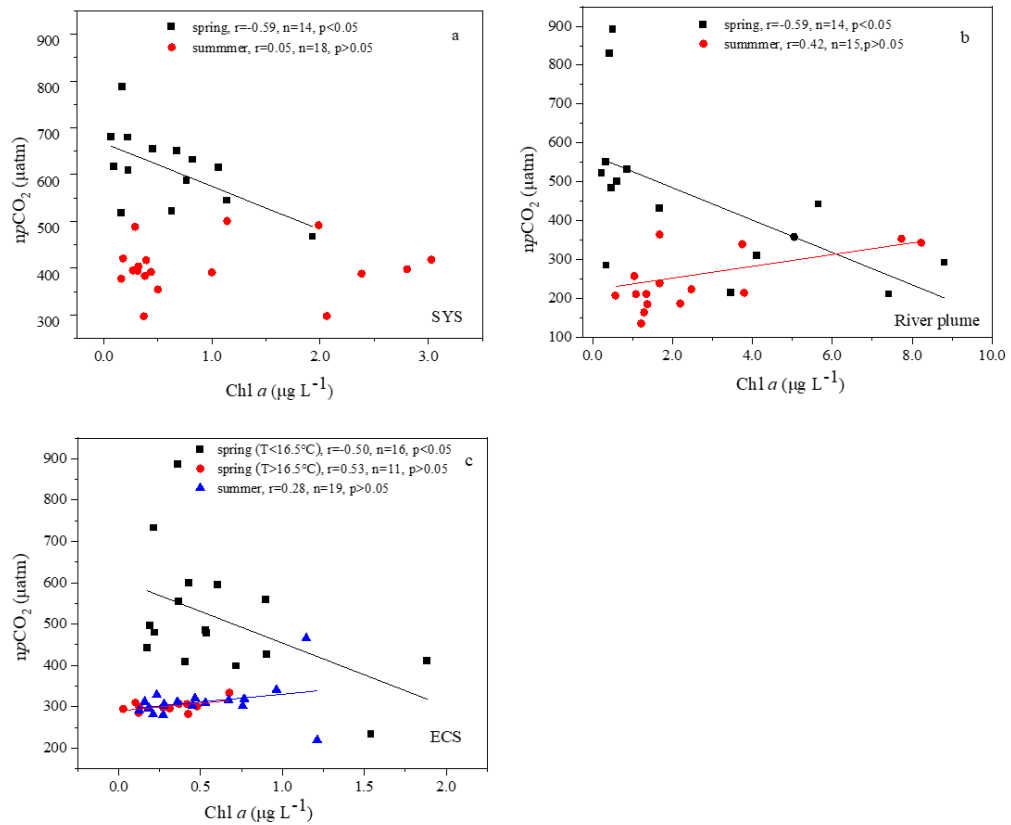
**Figure 10.** Relationship n$p$CO$_2$ and Chl $a$ in spring and summer in three water masses: SYS (a), River plume (b) and ECS offshore waters (c).

In the plume area, the relationship of underway $p$CO$_2$ and SST in spring is negative but random in summer, while the relationship of $p$CO$_2$ and salinity in spring is random but positive in summer (Figures 9c and 9d). In summer, the positive relationship between $p$CO$_2$ and salinity was similar to the result of the cruise in July 2007, which was found by Zhai and Dai (2009). Relatively high $p$CO$_2$ (Figure 9d) near the Changjiang River mouth (S= 24–26) was mainly subjected to the physical mixing effect. Moreover, photosynthesis was at a low level given the light limitation and strong vertical mixing in the turbid area in spite of high concentration nutrients

495    supply, therefore resulting in high $p\text{CO}_2$ distribution (He et al., 2013; Zhai et al.,

496    2007). Besides, this area was also more affected by the SYS through the Yellow Sea

497    Coastal Current in spring that carried higher $\text{CO}_2$ water southward, thereby resulting

498    in high $p\text{CO}_2$ in the northwest corner of the Changjiang estuary with moderate salinity

499    (Su, 1998). In the outer estuary, low $p\text{CO}_2$ values were distributed in the northeast of

500    the Changjiang estuary. It demonstrated in addition to the physical processes but

501    reinforcement of biological action also greatly affected $p\text{CO}_2$ dynamics. In the south

502    branch of the Changjiang estuary, on one hand, high primary production in this region

503    was fueled by abundant nutrients with the Changjiang River supply, thus leading to

504    biological $\text{CO}_2$ uptake and low $p\text{CO}_2$; On the other hand, the upwelling carrying

505    $\text{CO}_2$-rich water, which from the flow-northward TWC bottom water, mixed with the

506    surface water and thereby elevated $p\text{CO}_2$ (Wang et al., 2011b). Therefore, the

507    upwelling effect canceled out the intensive biological activity to some extent, then

508    resulting in $p\text{CO}_2$ of the south branch slightly higher than the northwest branch

509    (Figure 6).

510        In spring, the overall random relationship between $p\text{CO}_2$ and salinity as well as

511    the relatively narrow salinity range revealed a strong mixing in water column.

512    Moreover, the negative correlation between $p\text{CO}_2$ and SST in spring also suggested

513    that the water mixing between high-$p\text{CO}_2$/low-temperature river water and

514    low-$p\text{CO}_2$/high-temperature ECS water. As for Zhe-Min Coastal Current, intensive

515    primary production occurred with the high nutrients loading from the Changjiang

516    River leading to low $p\text{CO}_2$ values (He et al., 2013; Guo et al., 2015). The negative

517  relationship between n$p$CO$_2$ and Chl $a$ in spring (r = -0.59, n = 14, p < 0.05, Figure

518  10b) demonstrated that biological activity was also the main driver on the $p$CO$_2$

519  distribution.

520       All summer stations in the ECS were confined to the shelf break of the ECS,

521  while some spring stations were expanded to the outer shelf of the ECS, which was

522  influenced by the KC and open ocean to some extent. The southern and outer shelf of

523  ECS was characterized by warm and saline water with the influences of TWC and KC.

524  In spring, considering that the isotherm of 16.5 °C coincided with the depth contour

525  of 100m in the ECS, the relationship underway $p$CO$_2$ and SST in the ECS offshore

526  waters was divided into two parts to discuss (Figure 9e): one is the negative

527  correlation in the inner and middle shelves with SST < 16.5 °C ($r$ = -0.49, p < 0.001);

528  another is the significant positive correlation in the outer shelf with SST > 16.5 °C ($r$

529  = 0.74, p < 0.001). This indicated that the $p$CO$_2$ variation in the outer shelf of the ECS

530  was mainly dominated by temperature and the apparent coefficient of temperature

531  effect on surface seawater $p$CO$_2$ was 0.0584 °C$^{-1}$, which was higher than that of the

532  0.0423 °C$^{-1}$ determined for North Atlantic surface water by Takahashi et al. (1993).

533  This suggested that the temperature effect on seawater $p$CO$_2$ was enhanced by other

534  important processes (i.e. mixing with Kuroshio subsurface CO$_2$-rich water). Moreover,

535  the apparent temperature coefficient was similar to that in South Atlantic Bight

536  (0.058 °C$^{-1}$; Jiang et al., 2008), and higher than that in northern South China Sea

537  (0.024, 0.049 and 0.03 °C$^{-1}$ in spring, autumn and winter, respectively; Tseng et al.,

538  2007), and northern Yellow Sea (0.0205 °C$^{-1}$; Xu et al., 2016). In the inner and middle

539    shelves of the ECS, the combined influence of the physical mixing and the biological

540    activity masked the effects of temperature on the $pCO_2$ distribution. The negative

541    relationship between n$pCO_2$ and Chl $a$ ($r$ = -0.50, n = 16, p < 0.05) also showed that

542    the phytoplankton production mainly led to the $pCO_2$ variation in the inner and

543    middle shelves. Moreover, the positive correlation of the $pCO_2$ and salinity in spring

544    (Figure 9f) could be an evidence to affirm the intrusion of high salinity $CO_2$-rich KC

545    water to the ECS.

546

547    **4.4 Air-sea $CO_2$ fluxes in subregions and implication**

548    With the three subregions categorized in the South Yellow-East China Sea region,

549    the seasonality variation of both $pCO_2$ and air-sea $CO_2$ fluxes were found in each

550    individual region. Theoretically, the variation of the $CO_2$ flux was mainly attributed to

551    the variability in $\Delta pCO_2$ and wind speed (Jiang et al., 2008). In the present study, we

552    used the same reanalyzed monthly averaged wind speed from ECMWF to calculate

553    the $CO_2$ flux inside each cruise. Therefore, there was no spatial pattern in the

554    intra-seasonal variation of the wind speed and the flux difference was solely ascribed

555    to the $\Delta pCO_2$. Therefore, all above factors that influencing $pCO_2$ variability also

556    affected the distributions of $CO_2$ flux.

557    In this study, the SYS served as a $CO_2$ sink in early spring and a $CO_2$ source in

558    summer with the average air-sea $CO_2$ flux of -2.11 ± 4.57 and 2.35 ± 4.30 mmol m$^{-2}$

559    d$^{-1}$, respectively. This was in good agreement with the findings in the surveys of Xue

560    et al. (2011) and Qu et al. (2017). To be more specific, it was unquestionable that the

561 SYS served as a $CO_2$ sink in spring because of low temperature and spring bloom.

562 The trajectory of underway $pCO_2$ data clearly verified that spring $pCO_2$ in the SYS

563 was all undersaturated except for the Subei shoal in the southwest SYS (Figure 6).

564 However, in summer, a strong $CO_2$ sink in the SYS from the June gradually reduced

565 to a weak sink or source in July and further converted to an obvious $CO_2$ source in

566 August, according to the compilation of our data and the results from Qu et al. (2014,

567 2017). In the SYS, the outbreak of *Ulva prolifera* bloom between the April and June

568 every year absorbs a large amount of $CO_2$, which promotes the SYS to become a

569 temporary $CO_2$ sink in early summer (Van Alstyne et al., 2015), then the degradation

570 of the *U. prolifera* in the mid-July to late August also accelerate it to act as a $CO_2$

571 source (Deng et al., 2018). Therefore, the temporal changes of $pCO_2$ and $CO_2$ flux are

572 combined results from biological activity, the Changjiang River plume and the

573 upwelling of the Yellow Sea Cold Water. An exception is that the southeastern SYS

574 along the Korean coast was a net strong $CO_2$ sink during spring, summer and fall,

575 whereas it was a net weak source during winter (Choi et al., 2019). The sharp contrast

576 in $CO_2$ fluxes could be attributed to regional variations in magnitude and the

577 terrestrial influences, especially the influences of Changjiang and Yellow Rivers on

578 the western SYS in summer. In short, the factors affecting the $pCO_2$ distribution and

579 $CO_2$ flux, especially in summer, are complicated, and more detailed mechanisms for

580 these changes in summer need further intense investigation.

581     As a whole, the river plume region always acted as a $CO_2$ sink with the fluxes of

582 $-3.78 \pm 7.44$ and $-5.17 \pm 6.65$ mmol $m^{-2}$ $d^{-1}$ from spring to summer. The estimated

583    $CO_2$ flux in summer were close to those of Zhai and Dai (2009) (-8.8 ± 5.8 and -4.9 ±

584    4.0 mmol m$^{-2}$ d$^{-1}$ in spring and summer) and multiple observations by Guo et al. (2015)

585    (-10.7 ± 8.2 and -6.5 ± 10.7 mmol m$^{-2}$ d$^{-1}$ in spring and summer), whereas the $CO_2$

586    flux we calculated in spring was lower than those. It could be ascribed to the fact that

587    spring is the transitional season from winter to summer and the plume area is also the

588    transitional zone from the inland to the ECS. Thus, the magnitude of $CO_2$ flux

589    changes associated with many factors, including wind speed, biological activity and

590    river discharge, etc. Therefore, the estimated $CO_2$ fluxes in this study are reasonable

591    in comparison with the $CO_2$ fluxes in spring from multiple observations, such as those

592    of Zhai and Dai (2009) and Guo et al. (2015). As for the ECS, the northern ECS

593    always was a sink in both spring and summer, due to the jointly impacts of primary

594    production and Changjiang River input (Kim et al., 2013), while the southern ECS

595    shifted the $CO_2$ sink in spring to source in summer with the increasing intrusion of

596    KC and TWC in summer. Overall, the ECS offshore water was also a strong sink in

597    spring with an average $CO_2$ flux of -5.56 ± 3.12 mmol m$^{-2}$ d$^{-1}$. When it comes to

598    summer, it turned into a $CO_2$ source with the seasonal average $CO_2$ flux of 1.73 ± 3.05

599    mmol m$^{-2}$ d$^{-1}$, which might be due to the fact that high temperature in the ECS

600    offshore waters, especially in the southern ECS, contributed to the high $p$$CO_2$ and a

601    $CO_2$ source in summer. This is also in good consistency with the flux reported by Guo

602    et al. (2015) in summer.

603

604    **5 Conclusion**

605    Based on the hydrological and carbonate parameters observations with high

606    spatial resolution in the South Yellow-East China Sea region from spring and summer

607    cruises, the results showed that DIC and TA values decreased generally from

608    nearshore to offshore, moreover, the low TA and DIC values as well as high pH,

609    occurred in the river plume, especially in the Zhe-Min Coastal Current in spring. The

610    DIC and TA values in the SYS were higher than those in the ECS due to the Yellow

611    River with intensive carbonate weathering and erosion in the drainage basin. The

612    South Yellow Sea and East China Sea, as a whole, turned from an important $CO_2$ sink

613    in spring to a weak $CO_2$ source in summer, Specifically, the air-sea $CO_2$ flux

614    displayed large spatial and temporal variations in three subregions: $CO_2$ sinks in the

615    SYS and ECS offshore water converted into sources from spring to summer, while the

616    river plume always served as a $CO_2$ sink both in spring and summer. The controlling

617    factors of $p$CO$_2$ differ in different regions and seasons. In general, temperature and

618    biological activity were the primary drivers in controlling the $p$CO$_2$ variability in the

619    SYS, and primary production was more important than temperature in summer. For

620    the river plume area, $p$CO$_2$ distribution was largely controlled by physical mixing and

621    biological activity, which could be attributed to the Changjiang runoff with high

622    nutrients supply, while temperature was the dominant factor in the outer shelf of the

623    ECS as the high-temperature KC saline water always occupied in the region.

624        This study improved the understand of sea surface carbonate chemistry dynamics

625    in the two adjacent margin seas with different physical conditions and may also help

626    to better understand the chemical dynamics in many other marine systems. To better

627    understand the role of the continental shelf seas in the global carbon cycle, more

comprehensive surveys and researches of direct $p$CO$_2$ measurements in the entire

South Yellow Sea and East China Sea, especially the seasons (autumn and winter)

with weak primary production, are needed.

**References**

Bauer, J. E., Cai, W. J., Raymond, P. A., Bianchi, T. S., Hopkinson, C. S., & Regnier, P.
   A. (2013). The changing carbon cycle of the coastal ocean. *Nature*, 504(7478),
   61–70. https://doi.org/10.1038/nature12857

Borges, A. V., Delille, B., & Frankignoulle, M. (2005). Budgeting sinks and sources
   of CO$_2$ in the coastal ocean: Diversity of ecosystems counts. *Geophysical
   research letters*, 32(14), L14601. https://doi.org/10.1029/2005GL023053

Bozec, Y., Thomas, H., Elkalay, K., & de Baar, H. J. (2005). The continental shelf

pump for $CO_2$ in the North Sea-evidence from summer observation. Marine

Chemistry, 93(2-4), 131–147. https://doi.org/10.1016/j.marchem.2004.07.006

Cai, W. J. (2011). Estuarine and coastal ocean carbon paradox: $CO_2$ sinks or sites of

terrestrial carbon incineration? *Annual Review of Marine Science*, 3, 123–145.

https://doi.org/10.1146/annurev-marine-120709-142723

Cai, W. J., Dai, M. H., & Wang, Y. C. (2006). Air-sea exchange of carbon dioxide in

ocean margins: A province-based synthesis. *Geophysical Research Letters*,

33(12), L12603. https://doi.org/10.1029/2006GL026219

Cai, W. J., Dai, M. H., Wang, Y. C., Zhai, W. D., Huang, T., Chen, S. T., et al. (2004).

The biogeochemistry of inorganic carbon and nutrients in the Pearl River

estuary and the adjacent Northern South China Sea. *Continental Shelf

Research*, 24(12), 1301–1319. https://doi.org/10.1016/j.csr.2004.04.005

Cai, W. J., Hu, X. P., Huang, W. J., Jiang, L. Q., Wang, Y. C., Peng, T. H., & Zhang, X.

(2010). Alkalinity distribution in the western North Atlantic Ocean margins.

*Journal of Geophysical Research: Oceans*, 115(C8), C08014.

https://doi.org/10.1029/2009JC005482

Cai, W. J., Wang, Z. A., & Wang, Y. C. (2003). The role of marsh-dominated

heterotrophic continental margins in transport of $CO_2$ between the atmosphere,

the land-sea interface and the ocean. *Geophysical Research Letters*, 30(16),

1849. https://doi.org/10.1029/2003GL017633

Chen, C. T. A. (2003). New vs. export production on the continental shelf. *Deep Sea

Research Part II: Topical Studies in Oceanography*, 50(6–7), 1327–1333.

672        https://doi.org/10.1016/S0967-0645(03)00026-2

673    Chen, C. T. A. (2009). Chemical and physical fronts in the Bohai, Yellow and East

674        China seas. *Journal of Marine Systems*, 78(3), 394–410.

675        https://doi.org/10.1016/j.jmarsys.2008.11.016

676    Choi, Y., Kim, D., Cho, S., & Kim, T. W. (2019). Southeastern Yellow Sea as a sink

677        for atmospheric carbon dioxide. *Marine pollution bulletin*, 149, 110550.

678        https://doi.org/10.1016/j.marpolbul.2019.110550

679    Chou, W. C., Gong, G. C., Sheu, D. D., Hung, C. C., & Tseng, T. F. (2009). Surface

680        distributions of carbon chemistry parameters in the East China Sea in summer

681        2007. *Journal of Geophysical Research: Oceans*, 114, C07026.

682        https://doi.org/10.1029/2008JC005128

683    Chou, W. C., Gong, G. C., Tseng, C. M., Sheu, D. D., Hung, C. C., Chang, L. P., &

684        Wang, L. W. (2011). The carbonate system in the East China Sea in winter.

685        *Marine Chemistry*, 123(1–4), 44–55.

686        https://doi.org/10.1016/j.marchem.2010.09.004

687    Dai, M. H., Cao, Z. M., Guo, X. H., Zhai, W. D., Liu, Z. Y., Yin, Z. Q., et al. (2013).

688        Why are some marginal seas sources of atmospheric $CO_2$?. *Geophysical*

689        *Research Letters*, 40(10), 2154–2158. https://doi.org/10.1002/grl.50390

690    DeGrandpre, M. D., Olbu, G. J., Beatty, C. M., & Hammar, T. R. (2002). Air-sea $CO_2$

691        fluxes on the US Middle Atlantic Bight. *Deep sea research part II: Topical*

692        *studies in oceanography*, 49(20), 4355–4367.

693        https://doi.org/10.1016/S0967-0645(02)00122-4

694    Deng, X., Liu, T., Liu, C. Y., Liang, S. K., Hu, Y. B., Jin, Y. M., & Wang, X. C. (2018).

695    Effects of *Ulva prolifera* blooms on the carbonate system in the coastal waters

696    of Qingdao. *Marine Ecology Progress Series*, 605, 73–86.

697    https://doi.org/10.3354/meps12739

698    Dickson, A. G. (1994). Determination of dissolved oxygen in sea water by Winkler

699    titration. *WHP Operations and Methods*, 1–14.

700    Goyet, C., Millero, F. J., O'Sullivan, D. W., Eischeid, G., McCue, S. J., & Bellerby, R.

701    G. J. (1998). Temporal variations of $p$CO$_2$ in surface seawater of the Arabian

702    Sea in 1995. *Deep Sea Research Part I: Oceanographic Research Papers*,

703    45(4–5), 609–623. https://doi.org/10.1016/S0967-0637(97)00085-X

704    Guo, X. H., Zhai, W. D., Dai, M. H., Zhang, C., Bai, Y., Xu, Y., et al. (2015). Air-sea

705    CO$_2$ fluxes in the East China Sea based on multiple-year underway

706    observations. *Biogeosciences*, 12(18), 5495–5514.

707    https://doi.org/10.5194/bg-12-5495-2015

708    He, X., Bai, Y., Pan, D., Chen, C. T., Cheng, Q., Wang, D., & Gong, F. (2013).

709    Satellite views of the seasonal and interannual variability of phytoplankton

710    blooms in the eastern China seas over the past 14 yr (1998–2011).

711    *Biogeosciences*, 10(7), 4721–4739. https://doi.org/10.5194/bg-10-4721-2013

712    Huang, W. J., Wang, Y., & Cai, W. J. (2012). Assessment of sample storage techniques

713    for total alkalinity and dissolved inorganic carbon in seawater. *Limnology and*

714    *oceanography: Methods*, 10(9), 711–717.

715    https://doi.org/10.4319/lom.2012.10.711

716  Isobe, A., & Matsuno, T. (2008). Long-distance nutrient-transport process in the

717      Changjiang river plume on the East China Sea shelf in summer. *Journal of*

718      *Geophysical      Research:      Oceans*,      113,      C04006.

719      https://doi.org/10.1029/2007JC004248

720  Jiang, L. Q., Cai, W. J., Wanninkhof, R., Wang, Y., & Lüger, H. (2008). Air-sea $CO_2$

721      fluxes on the US South Atlantic Bight: Spatial and seasonal variability.

722      *Journal    of    Geophysical    Research:    Oceans*,    113,    C07019.

723      https://doi.org/10.1029/2007JC004366

724  Jiang, Z. P., Tyrrell, T., Hydes, D. J., Dai, M., & Hartman, S. E. (2014). Variability of

725      alkalinity and the alkalinity-salinity relationship in the tropical and subtropical

726      surface   ocean.   *Global   Biogeochemical   Cycles*,   28(7),   729 – 742.

727      https://doi.org/10.1002/2013GB004678

728  Jin, J., Liu, S. M., Ren, J. L., Liu, C. G., Zhang, J., & Zhang, G. L. (2013). Nutrient

729      dynamics and coupling with phytoplankton species composition during the

730      spring blooms in the Yellow Sea. *Deep Sea Research Part II: Topical Studies*

731      *in Oceanography*, 97, 16–32. https://doi.org/10.1016/j.dsr2.2013.05.002

732  Kempe, S., & Pegler, K. (1991). Sinks and sources of $CO_2$ in coastal seas: the North

733      Sea. *Tellus                        B*, 43(2),                        224–235.

734      https://doi.org/10.1034/j.1600-0889.1991.00015.x

735  Kim, D., Choi, S. H., Shim, J., Kim, K. H., & Kim, C. H. (2013). Revisiting the

736      Seasonal Variations of Sea-Air $CO_2$ Fluxes in the Northern East China Sea.

737      *Terrestrial,    Atmospheric    &    Oceanic    Sciences*,    24(3),    409-419.

738        https://doi.org/10.3319/TAO.2012.12.06.01(Oc)

739    Lee, H. J., & Chao, S. Y. (2003). A climatological description of circulation in and

740        around the East China Sea. *Deep Sea Research Part II: Topical Studies in*

741        *Oceanography*, 50(6–7), 1065–1084.

742        https://doi.org/10.1016/S0967-0645(03)00010-9

743    Li, W., Wang, Y. H., Wang, J. N., & Wei, H. (2012). Distributions of water masses and

744        hydrographic structures in the Yellow Sea and East China Sea in spring and

745        summer 2011. *Oceanologia et Limnologia Sinica*, 3, 615–623. (In Chinese

746        with English abstract)

747    Li, Y., Yang, X., Han, P., Xue, L., & Zhang, L. (2017). Controlling mechanisms of

748        surface partial pressure of $CO_2$ in Jiaozhou Bay during summer and the

749        influence of heavy rain. *Journal of Marine Systems*, 173, 49–59.

750        https://doi.org/10.1016/j.jmarsys.2017.04.006

751    Liu, C., Zhang, C., Yang, X., Gong, H., & Zhang, Z. (2008). A multilayer study of

752        *p*$CO_2$ in the surface waters of the Yellow and South China Seas in spring and

753        the sea-air carbon dioxide flux. *Journal of Ocean University of China*, 7(3),

754        263–268. https://doi.org/10.1007/s11802-007-0263-2

755    Liu, X., Huang, B., Huang, Q., Wang, L., Ni, X., Tang, Q., et al. (2015). Seasonal

756        phytoplankton response to physical processes in the southern Yellow Sea.

757        *Journal of Sea Research*, 95, 45–55.

758        https://doi.org/10.1016/j.seares.2014.10.017

759    Liu, Z., Zhang, L., Cai, W. J., Wang, L., Xue, M., & Zhang, X. (2014). Removal of

760     dissolved inorganic carbon in the Yellow River Estuary. *Limnology and*

761     *oceanography*, 59(2), 413–426. https://doi.org/10.4319/lo.2014.59.2.0413

762  Mackenzie, F. T., Bewers, J. M., Charlson, R. J., Hofmann, E. E., Knauer, G. A., Kraft,

763     J. C., et al. (1991). What is the importance of ocean margin processes in global

764     change?. *in Ocean Margin Processes in Global Change*, editedby R. F. C.

765     Mantoura, J. M. Martin, and R. Wollast, pp. 433–454, JohnWiley, New York,

766     1991. https://doi.org/10013/epic.12626

767  Millero, F. J. (1995). Thermodynamics of the carbon dioxide system in the oceans.

768     *Geochimica et Cosmochimica Acta*, 59(4), 661–677.

769     https://doi.org/10.1016/0016-7037(94)00354-O

770  Omar, A. M., Olsen, A., Johannessen, T., Hoppema, M., Thomas, H., & Borges, A. V.

771     (2010). Spatiotemporal variations of $f$CO$_2$ in the North Sea. *Ocean Science*.

772     6(1), 77–89. http://dx.doi.org/10.5194/os-6-77-2010

773  Parsons, T. R., Maita, Y., & Lalli, C. M. (1984). Amanual of chemical and biological

774     methods for seawater analysis. *Oxford: Pergamon*, 1, 173.

775  Pierrot, D., Neill, C., Sullivan, K., Castle, R., Wanninkhof, R., Lüger, H., et al. (2009).

776     Recommendations for autonomous underway $p$CO$_2$ measuring systems and

777     data-reduction routines. *Deep Sea Research Part II: Topical Studies in*

778     *Oceanography*, 56(8–10), 512–522. https://doi.org/10.1016/j.dsr2.2008.12.005

779  Qi, J., Yin, B., Zhang, Q., Yang, D., & Xu, Z. (2014). Analysis of seasonal variation of

780     water masses in East China Sea. *Chinese Journal of Oceanology and*

781     *Limnology*, 32(4), 958–971. https://doi.org/10.1007/s00343-014-3269-1

782  Qian, W., Chen, Y., Yang, L. M., Peng., Y. Z., Zhang, L., Li, T. Y., & Jiang, M. H.

783      (2019). Carbon Fraction and Fluxes in the Lower Reach of Minjiang River.

784      Research of Environmental Sciences, 32(4), 648–653. (In Chinese with

785      English abstract)

786  Qu, B., Song, J., Yuan, H., Li, X., & Li, N. (2014). Air-sea $CO_2$ exchange process in

787      the southern Yellow Sea in April of 2011, and June, July, October of 2012.

788      *Continental        Shelf        Research*,        80,        8–19.

789      https://doi.org/10.1016/j.csr.2014.02.001

790  Qu, B., Song, J., Yuan, H., Li, X., Li, N., & Duan, L. (2017). Comparison of

791      carbonate parameters and air-sea $CO_2$ flux in the southern Yellow Sea and East

792      China Sea during spring and summer of 2011. *Journal of Oceanography*,

793      73(3), 365–382. https://doi.org/10.1007/s10872-016-0409-6

794  Qu, B., Song, J., Yuan, H., Li, X., Li, N., Duan, L., et al. (2015). Summer carbonate

795      chemistry dynamics in the Southern Yellow Sea and the East China Sea:

796      Regional variations and controls. *Continental Shelf Research*, 111, 250–261.

797      https://doi.org/10.1016/j.csr.2015.08.017

798  Song, J., Qu, B., Li, X., Yuan, H., Li, N., & Duan, L. (2018). Carbon sinks/sources in

799      the Yellow and East China Seas—Air-sea interface exchange, dissolution in

800      seawater, and burial in sediments. *Science China Earth Sciences*, 61(11),

801      1583-1593. https://doi.org/10.1007/s11430-017-9213-6

802  Su, J., (1998). Circulation dynamics of the China Seas north of 18°N. The sea, 11,

803      483-505.

Takahashi, T., Olafsson, J., Goddard, J. G., Chipman, D. W., & Sutherland, S. C. (1993). Seasonal variation of $CO_2$ and nutrients in the high-latitude surface oceans: A comparative study. *Global Biogeochemical Cycles*, 7(4), 843–878. https://doi.org/10.1029/93GB02263

Takahashi, T., Sutherland, S. C., Sweeney, C., Poisson, A., Metzl, N., Tilbrook, B., et al. (2002). Global sea-air $CO_2$ flux based on climatological surface ocean $pCO_2$, and seasonal biological and temperature effects. *Deep Sea Research Part II: Topical Studies in Oceanography*, 49(9–10), 1601–1622. https://doi.org/10.1016/S0967-0645(02)00003-6

Takahashi, T., Sutherland, S. C., Wanninkhof, R., Sweeney, C., Feely, R. A., Chipman, D. W., et al. (2009). Climatological mean and decadal change in surface ocean $pCO_2$, and net sea-air $CO_2$ flux over the global oceans. *Deep Sea Research Part II: Topical Studies in Oceanography*, 56(8–10), 554–577. https://doi.org/10.1016/j.dsr2.2008.12.009

Thomas, H., Bozec, Y., de Baar, H. J., Borges, A., & Schiettecatte, L. S. (2005). Controls of the surface water partial pressure of $CO_2$ in the North Sea. *Biogeosciences*, 2(4), 323–334. https://doi.org/10.5194/bg-2-323-2005

Tseng, C. M., Wong, G. T. F., Chou, W. C., Lee, B. S., Sheu, D. D., & Liu, K. K. (2007). Temporal variations in the carbonate system in the upper layer at the SEATS station. *Deep Sea Research Part II: Topical Studies in Oceanography*, 54(14–15), 1448–1468. https://doi.org/10.1016/j.dsr2.2007.05.003

Tsunogai, S., Watanabe, S., & Sato, T. (1999). Is there a "continental shelf pump" for

826    the absorption of atmospheric $CO_2$?. *Tellus B: Chemical and Physical*

827    *Meteorology*, 51(3), 701–712. https://doi.org/10.3402/tellusb.v51i3.16468

828    Van Alstyne, K. L., Nelson, T. A., & Ridgway, R. L. (2015). Environmental chemistry

829    and chemical ecology of "green tide" seaweed blooms. *Integrative and*

830    *comparative biology*, 55(3), 518–532. https://doi.org/10.1093/icb/icv035

831    Wang, B., Chen, J. F., Jin, H. Y., Li, H. L., Liu, X. Z., Zhuang, Y. P., et al. (2011).

832    Preliminary study on the dissolved inorganic carbon system and its response

833    mechanism in Changjiang River Estuary and its adjacent sea areas in summer.

834    *Journal of Marine Science*, 29, 63–70. (In Chinese with English abstract)

835    Wang, S. L., Chen, C. T. A., Hong, G. H., & Chung, C. S. (2000). Carbon dioxide and

836    related parameters in the East China Sea. *Continental Shelf Research*, 20(4–5),

837    525–544. https://doi.org/10.1016/S0278-4343(99)00084-9

838    Wang, X. H., Qiao, F., Lu, J., & Gong, F. (2011). The turbidity maxima of the

839    northern Jiangsu shoal-water in the Yellow Sea, China. *Estuarine, Coastal and*

840    *Shelf Science*, 93(3), 202–211. https://doi.org/10.1016/j.ecss.2010.10.020

841    Wang, B., & Wang, X. (2007). Chemical hydrography of coastal upwelling in the East

842    China Sea. *Chinese Journal of Oceanology and Limnology*, 25(1), 16–26.

843    https://doi.org/10.1007/s00343-007-0016-x

844    Wanninkhof, R. (2014). Relationship between wind speed and gas exchange over the

845    ocean revisited. *Limnology and Oceanography: Methods*, 12(6), 351–362.

846    https://doi.org/10.4319/lom.2014.12.351

847    Weiss, R. F. (1974). Carbon dioxide in water and seawater: the solubility of a

848      non-ideal gas. *Marine chemistry*, 2(3), 203–215.

849      https://doi.org/10.1016/0304-4203(74)90015-2

850      Weiss, R. F., & Price, B. A. (1980). Nitrous oxide solubility in water and seawater.

851      *Marine chemistry*, 8(4), 347–359.

852      https://doi.org/10.1016/0304-4203(80)90024-9

853      Wu, H., Shen, J., Zhu, J., Zhang, J., & Li, L. (2014). Characteristics of the Changjiang

854      plume and its extension along the Jiangsu Coast. *Continental Shelf Research*,

855      76, 108–123.

856      Xu, X., Zang, K., Huo, C., Zheng, N., Zhao, H., Wang, J., & Sun, B. (2016).

857      Aragonite saturation state and dynamic mechanism in the southern Yellow Sea,

858      China. *Marine pollution bulletin*, 109(1), 142–150.

859      https://doi.org/10.1016/j.marpolbul.2016.06.009

860      Xue, L., Zhang, L., Cai, W. J., & Jiang, L. Q. (2011). Air-sea $CO_2$ fluxes in the

861      southern Yellow Sea: An examination of the continental shelf pump hypothesis.

862      *Continental Shelf Research*, 31(18), 1904–1914.

863      https://doi.org/10.1016/j.csr.2011.09.002

864      Zhai, W. D., Chen, J. F., Jin, H. Y., Li, H. L., Liu, J. W., He, X. Q., & Bai, Y. (2014).

865      Spring carbonate chemistry dynamics of surface waters in the northern East

866      China Sea: Water mixing, biological uptake of $CO_2$, and chemical buffering

867      capacity. *Journal of Geophysical Research: Oceans*, 119(9), 5638–5653.

868      https://doi.org/10.1002/2014JC009856

869      Zhai, W. D., & Dai, M. H. (2009). On the seasonal variation of air-sea $CO_2$ fluxes in

870    the outer Changjiang (Yangtze River) Estuary, East China Sea. Marine

871    Chemistry, 117(1–4), 2–10. https://doi.org/10.1016/j.marchem.2009.02.008

872  Zhai, W. D., Dai, M. H., & Guo, X. H. (2007). Carbonate system and $CO_2$ degassing

873    fluxes in the inner estuary of Changjiang (Yangtze) River, China. *Marine*

874    *chemistry*, 107(3), 342–356. https://doi.org/10.1016/j.marchem.2007.02.011

875  Zhang, J., Huang, W. W., Liu, M. G., & Zhou, Q. (1990). Drainage basin weathering

876    and major element transport of two large Chinese rivers (Huanghe and

877    Changjiang). *Journal of Geophysical Research: Oceans*, 95(C8),

878    13277–13288. https://doi.org/10.1029/JC095iC08p13277

879  Zhang, L., Xue, L., Song, M., & Jiang, C. (2010). Distribution of the surface partial

880    pressure of $CO_2$ in the southern Yellow Sea and its controls. *Continental Shelf*

881    *Research*, 30(3–4), 293–304. https://doi.org/10.1016/j.csr.2009.11.009